A MULTIBODY APPROACH TO THE ANALYSIS OF HELICOPTER-TERRAIN INTERACTION

Stefania Gualdi, Pierangelo Masarati†, Marco Morandini, and Gian Luca Ghiringhelli
Dipartimento di Ingegneria Aerospaziale, Politecnico di Milano,
via La Masa 34, 20156 Milano, Italy

Abstract

The paper presents an analysis of the significant aspects related to the interaction between rotorcrafts and the terrain. It addresses the analysis of a typical medium weight helicopter, with detailed wheel landing gear and full rotor dynamics, during significant maneuvers. The aim of this work is in fact, on one hand, to investigate the interaction between the landing devices and the terrain under realistic conditions, such as those obtained by simultaneously modeling the dynamics of the helicopter rotor. On the other hand, it is aimed at analyzing the effects of realistic ground loads on the rotor components. The validity of the multibody/multidisciplinary approach for this kind of problems is discussed.

Acronyms	
MLG	main landing gear
NLG	nose landing gear
p.u.l.	per unit length
SR	(tire) slip ratio

Symbols	
a, b	tire elliptic footprint axes
A_h	shock absorber hydraulic area
A_o	shock absorber orifice area
A_s	shock absorber gas area
A_t	tire footprint area
C_d	orifice discharge coefficient
C_i	gas stroke ratio
F_e	shock absorber elastic force
F_f	shock absorber friction force
F_v	shock absorber viscous force
$F_{x,y}$	tire longitudinal and lateral forces
F_z	tire normal force
l	tire vertical deflection
p_{s_0}	shock absorber gas reference pressure
p_t	tire internal pressure
p_{t_0}	tire reference internal pressure
R_t	tire radius
r_t	tire torus internal radius
s	shock absorber stroke
u	rotor induced velocity
v_a	wheel axle velocity
V_{s_0}	shock absorber gas reference volume
V_{t_0}	tire reference volume
v_{th}	tire velocity threshold
α	tire slip angle
γ_s	shock absorber polytropic exponent
γ_t	tire polytropic exponent
μ	generic friction coefficient
ρ	hydraulic fluid density
ω_t	tire angular velocity

Introduction

The interaction between rotorcrafts and the terrain is a complex problem because it involves many different aspects of rotorcraft analysis and design. Typical problems of non-trivial helicopter interaction with the ground are represented by hard landings, fast taxiing over an obstacle or in the presence of shimmy, detailed analysis of the ground resonance phenomenon, including the effects of large displacements and rotations, aerodynamic loads and nonlinear damping and constitutive effects in general (which are usually neglected in conventional analyses). In fact, the problem is typically nonlinear due to the presence of configuration dependent nonlinearities such as those related to finite displacements and rotations as well as constitutive nonlinearities, intrinsic in landing gear elements (tires, shock absorbers) and due to friction.
Linear (and linearized) models present a series of limitations due to the excessive simplifications that have to be adopted: some of the above mentioned nonlinearities are hardly linearizable, e.g. friction; others limit the applicability of the analysis to local stability considerations. Moreover, linearized models are difficult to adapt to analyses situated far from the reference design point.

†Corresponding author,
Tel.: +39 02 2399 8309
Fax: +39 02 2399 8334
E-mail: *pierangelo.masarati@polimi.it*

Presented at the European Rotorcraft Forum 2002
Bristol (UK) 17–20 September 2002

Multibody Analysis

The need to account for large rotations and displacements naturally leads to the use of multibody analysis codes. This is particularly true for helicopters; in fact great impulse to the development of these instruments originated from the needs of (flexible) rotor dynamics and aeroelasticity [1, 2]. The multibody approach allows the use of modular models to build a complete system with the required detail for each subpart. As a result, the same model (or common components) can be used for the different analyses that are required at each stage of development. One of the most significant features is that kinematics have an exact formulation within the chosen idealization of the real system. The typical use involves time step integration of dynamic system behavior; as a result, the potential becomes that of a virtual prototyping system. An example of an exhaustive application could be the complete simulation of helicopter ground resonance including the interacting effects of all the above mentioned nonlinearities, complete airframe flexibility and rotor aerodynamics. Multibody analysis is widely used in the aerospace industry; in the field of ground handling analysis, for example, commercial codes such as Adams, Mecano, Simpack and other software have been successfully applied (e.g. [3, 4, 5, 6, 7]; a large literature on the subject is available).

While commercial multibody analysis codes gained an appreciable maturity, the need for special features and the possibility to interact with the code at inner levels led our research team at the "Dipartimento di Ingegneria Aerospaziale" of the University "Politecnico di Milano" to the development of the Open Source software MBDyn (available at the URL `http://www.aero.polimi.it/~mbdyn`), which proved very effective and scalable in multidisciplinary rotorcraft analysis [2, 8, 9].

Our multibody rotorcraft analysis focused essentially on rotor dynamics and aeroservoelasticity. Recently, the code was employed for ground handling analysis of fixed wing aircraft. Particular attention was dedicated to the validation of the results with data from drop test experiments conducted over years of activity at the "Dipartimento di Ingegneria Aerospaziale" in landing gear research and, recently, certification [10]. Its carry over to the rotating wing field is a natural prosecution of that work.

In a multibody environment, the landing gear configuration in terms of geometry, inertial characteristics and kinematics, however complex, can be fairly easily modeled with the appropriate parts and joints. For functional components such as shock absorbers and tires though, one must resort to more or less complex analytical models, depending on the phenomena to be simulated and the accuracy desired. In fact, the major difficulties encountered while modeling the dynamic behavior of a landing gear during impact and ground manoeuvring are essentially due to the nonlinearities introduced by the presence of tires and shock absorbers. Once the landing gear subsystem is modeled and validated, it can be integrated in the complete rotorcraft model and landing and ground manoeuvre simulations can be performed. This allows the designer to investigate rotorcraft performance in landing and ground handling over a wide range of operational configurations.

Model Description

The model considered in this work is composed of two main elements: (a) the landing gear, and (b) the rotor. These components are detailed in order to model the dynamic properties that are essential in this work. There are other significant parts that would require additional substructuring and detailed analysis, e.g. the flexibility of the airframe, the tail rotor dynamics, the control system hydraulics and so on; in the present case, only the interaction between main rotor and landing gear dynamics will be considered.

The landing gear is described first.

Landing Gear Layout The overall geometry of the helicopter is presented in Figure 1. A typical tricycle wheel landing gear has been modeled. A telescopic strut was chosen for the nose landing gear (NLG) while the main landing gear (MLG) was represented by a classical trailing link layout. The basic components considered for each gear are the structural cylinder, the nonlinear oleopneumatic shock absorber, the fork, the wheel, and the attachment braces (i.e. the actual interface towards the fuselage). Correct kinematic behavior is guaranteed by suitable joint orientation. The estimated landing gear mass is distributed among the parts and beam characteristics are assigned referring to a typical landing gear layout.

The modeling of the landing gear structural components is straightforward within the MBDyn code, while special attention must be dedicated to the nonlinear shock absorber and tire models.

Shock Absorber The nonlinear oleopneumatic shock absorber model is implemented using a rod element with a particular viscoelastic constitutive law. The elastic and viscous force components are modeled using the classical [11] polytropic compression and

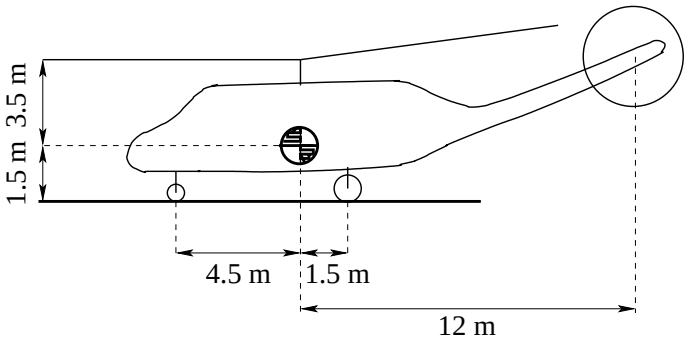

Figure 1: Helicopter layout; MLG track is 3.5 m

velocity-squared damping equations (1, 2):

$$F_e = A_s p_{s_0} \left(\frac{V_{s_0}}{V_{s_0} - C_i A_s s} \right)^{\gamma_s} \quad (1)$$

$$F_v = \frac{1}{2} \rho A_h^3 \frac{|\dot{s}| \, \dot{s}}{A_o^2 C_d^2} \quad (2)$$

Both the variation of gas chamber volume and the orifice area (in the presence of metering pins) are a function of the shock absorber stroke, s. The latter may also depend on the direction of shock-absorber motion, $\dot{s}/|\dot{s}|$, (compression or extension). The friction between cylinder and piston is accounted for by adding a contribution F_f that is proportional to the elastic force of Equation (1) and opposed to the motion:

$$F_f = \mu \tanh \left(\frac{\dot{s}}{\dot{s}_{ref}} \right) F_e$$

The hyperbolic tangent term guarantees continuity when passing through $\dot{s} = 0$.

Tire The tire model implemented in MBDyn is an evolution of the GRAALL model, specifically developed at Politecnico di Milano for landing impact analysis [10]. The GRAALL model adopts a physical approach, with the vertical force:

$$F_z = A_t p_t \left(1 + \tanh \left(\frac{\dot{l}}{\dot{l}_{ref}} \right) \right) \quad (3)$$

calculated using a polytropic compression

$$p_t = p_{t_0} \left(\frac{V_{t_0}}{V_{t_0} - A_t l/2} \right)^{\gamma_t}$$

based on the intersection volume of a torus with the ground, in a simplified form:

$$A_t = 3.7 ab \frac{l}{R_t}$$

yielding a nonlinear vertical stiffness. The hyperbolic tangent term is used to model tire hysteresis, using a reference normal tire deflection rate, $\dot{l}_{ref}$. The terrain in this case is considered infinitely rigid; in case of soft soil, the interaction volume can be approximated considering a polytropic compression of the terrain. The tire longitudinal and lateral force components depend on contact point slip ratio and side slip angle, respectively defined as:

$$\mathrm{SR} = \frac{\left| (v_a + \omega_t (R_t - l))_{long.} \right|}{\left| (v_a)_{long.} \right| + v_{th_{\mathrm{SR}}}}$$

where the instantaneous radius, $R_t - l$, is considered, and:

$$\alpha = \mathrm{atan} \left(\frac{(v_a)_{lat.}}{(v_a)_{long.}} \right) \tanh^2 \left(\frac{|v_a|}{v_{th_\alpha}} \right)$$

A modified form of the usual SR is used to ensure the correct behavior of the tire model in every situation that may occur during a transient response, including drop tests with wheel pre-spin, when the angular speed of the wheel and the velocity of the axle can vary from zero to a finite value, without incurring in singularities. The forces have the following expressions:

$$\begin{aligned} F_x &= \mu_{long.}(\mathrm{SR}, \alpha) F_z \\ F_y &= \mu_{lat.}(\mathrm{SR}, \alpha) F_z \end{aligned}$$

An essentially vertical contact is assumed, i.e. the axle of the wheel is parallel to the ground. In case of cambered contact, appropriate corrections must be used. They are not detailed because their use is limited in helicopter landing analysis.

Landing Gear Parameters The physical and geometrical parameters which appear in the shock absorber constitutive law, Equation (2), were chosen referring to typical landing gear data, adjusting the values in

Table 1: Shock Absorber Properties

γ_s	1.30	
C_d	0.70	
ρ	900.00	Kg/m^3
μ	0.10	
$\dot{s}_{ref}$	2.50e−2	m/s
Main Landing Gear		
A_s	6.65e−3	m^2
A_h	6.40e−3	m^2
A_o for $\dot{s} < 0$	6.50e−5	m^2
A_o for $\dot{s} > 0$	3.00e−5	m^2
C_i	1.00	
p_{s_0}	2.10e+6	Pa
V_{s_0}	1.60e−3	m^2
Nose Landing Gear		
A_s	2.90e−3	m^2
A_h	6.10e−3	m^2
A_o for $\dot{s} < 0$	4.50e−5	m^2
A_o for $\dot{s} > 0$	1.50e−5	m^2
C_i	1.07	
p_{s_0}	9.84e+5	Pa
V_{s_0}	8.00e−4	m^2

order to fulfill FAR/JAR 29 drop test requirements [12, 13]. Both NLG and MLG shock absorbers are equipped with metering pins and direction-dependent fixed orifice areas. The tire parameters, estimated using consolidated design procedures [14], have been chosen referring once again to typical landing gear design data for 450x140-8 and 670x210-12 tires. The tire-terrain friction coefficients are those relative to smooth asphalt [15]. The shock absorber parameters for both the MLG and NLG are listed in Table 1. Figure 2 shows the shock absorber orifice areas at different strokes, due to the variable section metering pin. The effective orifice area is the sum of this term and the fixed orifice area A_o reported in Table 1. Figures 3 and 4 show the simulated MLG and NLG shock absorber characteristic curve for limit drop tests. The drop height (8 in., corresponding to about 0.20 m) results in a touchdown vertical speed of 2.0 m/s. The equivalent mass used for each landing gear accounted for 2/3 of the thrust at maximum take-off weight (FAR/JAR 29). Table 2 shows the MLG and NLG tire parameters, while Figure 5 shows the characteristics of the tires. Figures 6-7 show a qualitative form of the tire slip coefficients as functions of the slip ratio SR and of the slip angle α [16, 17].

Rotor The rotor is representative of a generic medium

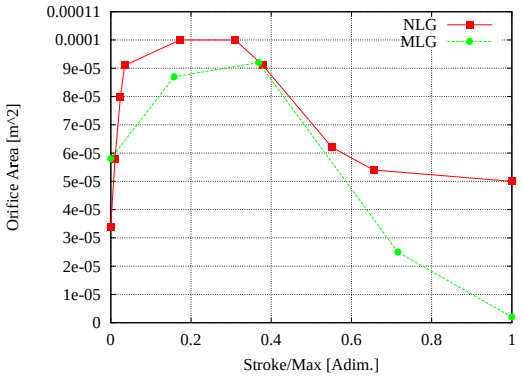

Figure 2: Dependence of orifice area on stroke of MLG and NLG shock absorbers due to variable section metering pins (MLG $s_{\max} = 0.2$ m, NLG $s_{\max} = 0.29$ m)

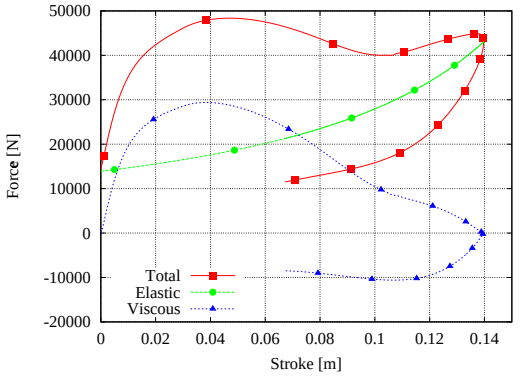

Figure 3: MLG shock absorber characteristics

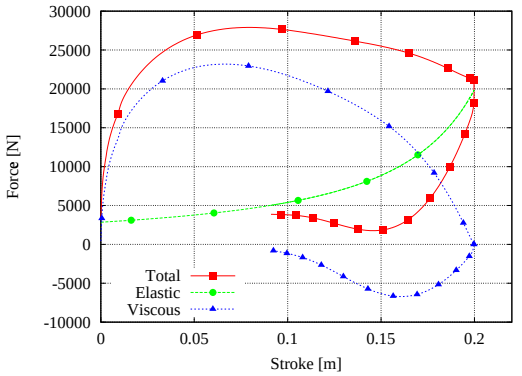

Figure 4: NLG shock absorber characteristics

Table 2: Tire Properties		
$\dot{l}_{ref}$	30.0	m/s
$v_{th_{\mathrm{SR}}}$	5.0	m/s
v_{th_α}	0.05	m/s
γ_t	1.3	

Main Landing Gear		
p_{t_0}	1.3e+6	Pa
R_t	0.335	m
r_t	0.105	m

Nose Landing Gear		
p_{t_0}	1.035e+6	Pa
R_t	0.2235	m
r_t	0.0705	m

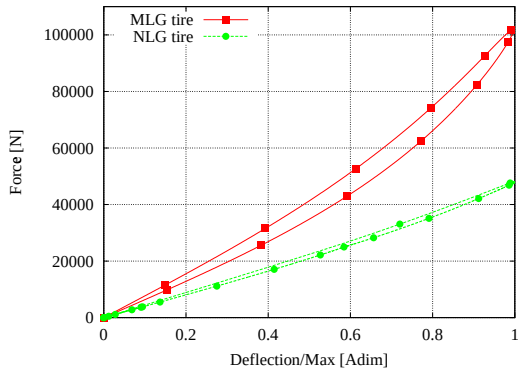

Figure 5: MLG and NLG tire characteristics

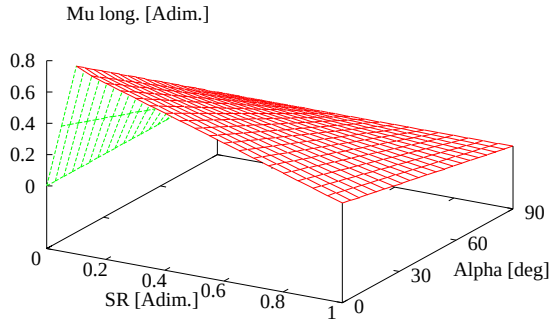

Figure 6: Tire longitudinal friction coefficient

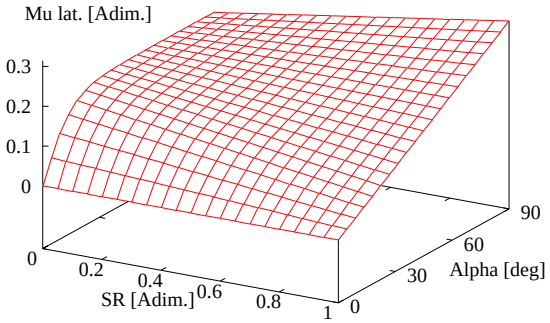

Figure 7: Tire lateral friction coefficient

Table 3: Rotor Properties		
Number of blades, n_b	5	
Radius, R	8.0	m
Cut-out, R_0	1.66	m
Chord, c	0.5	m
Angular velocity, Ω	25.0	rad/s
Hinge offset, e	0.2	m
Pitch-flap coupling, δ_3	0.0	deg
Root pitch stiffness, K_θ	10.0	N/rad
Root flap stiffness, K_β	100.0	N/rad
Root lag stiffness, K_ξ	100.0	N/rad
Pitch link stiffness, $M_{c/\theta}$	1.6e5	Nm/rad
Lag damper, $M_{\xi/\dot{\xi}}$	1.e4	Nm/rad/s
Blade mass p.u.l., m	10.0	Kg/m
Blade inertia p.u.l., J_p	1.28	Kgm
Blade twist, θ	-12.0	deg
Twist stiffness, GJ	1.8e6	Nm^2
Beam stiffness, EJ_y	1.5e5	Nm^2
Chord stiffness, EJ_z	1.0e7	Nm^2

weight helicopter; its essential properties are detailed in Table 3. The properties of the blades are uniform along the span; the elastic, the inertial and the aerodynamic axes are coincident, and lie on the pitch change axis at 25% of the blade chord, c. This simple layout has been chosen to allow an easy reproduction of the results and to avoid the influence of coupling terms on the dynamic properties of the rotor; however, more sophisticated geometries and mechanical properties can be easily accounted for by the proposed approach, with an appreciable generality. The blade is attached to the hub by an elastomeric bearing, represented by rotational springs about pitch (K_θ), flap (K_β), and lag (K_ξ) axes (no damping in the elastomeric bearing is considered in this work). A lag damper is attached at the rear of the blade, and is modeled by means of a viscoelastic rod with equivalent damping ratio $M_{\xi/\dot{\xi}}$. The blade pitch is constrained to the position and orientation of a swashplate by means of a pitch link with equivalent pitch stiffness $M_{c/\theta}$. These effects are

Table 4: Rotor Dynamic Properties

Mode	1/rev
1^{st}lag	0.20
1^{st}flap	1.01
2^{nd}flap	2.79
1^{st}twist	4.54
3^{rd}flap	5.65

Table 5: Helicopter Properties

Overall mass, M	9500.0	kg
Overall length, L	20.0	m
Roll Inertia, I_x	3000.0	kg m^2
Pitch Inertia, I_y	15000.0	kg m^2
Yaw Inertia, I_z	15000.0	kg m^2
Roll frequency	1.0	Hz
Pitch frequency	3.0	Hz

introduced in the multibody model by means of elements that reproduce the corresponding physical components; as a consequence, all the above mentioned properties are allowed to change when the system departs from the design point because of the inherently nonlinear geometry of the blade constraints and of the control system kinematics. The blade pretwist goes from 9 deg at the root to -3 deg at the tip. The rotor blades are modeled by means of an original finite volume scheme based on an "intrinsic" or "exact" beam formulation, which implicitly accounts for the geometric stiffness [18]. The inertia forces, including the centrifugal and *Coriolis* effects, are applied to the beams by the rigid bodies in a thoroughly consistent manner, so there is no approximation of the blade rotation except for the spatial discretization. The dynamic properties of the resulting system are listed in Table 4. The frequencies of the modes are not affected by the aerodynamics because there is no coupling between pitch, flap and lag in the reference configuration. The aerodynamics are modeled by means of a classical strip theory with tabulated aerodynamic coefficients spanning 360 degrees of pitch and $0 \div 0.9$ Mach number, with corrections for unsteady flow, dynamic stall, and radial flow drag; dynamic inflow is considered as well.

Airframe and Other Parts In the present work, the airframe is modeled as a single rigid body. A flexible model, possibly based on a flexible superelement, would definitely enhance the analysis: it is in fact reasonable to assume that in hard landing conditions the fuselage deflection is appreciable. This feature is indeed supported by the code, however it is not essential for the purpose of this work; moreover, no specific data was available at the time the work was carried out.

The tail rotor is modeled by a concentrated force, applied 12 m behind the main rotor mast and at the same height as the main rotor hub. The force balances the main rotor torque exactly and depends linearly on the yaw velocity to damp the yaw motion. This is deemed sufficient, because the trimming of a complete helicopter is beyond the purpose of this work. The main properties of the helicopter are listed in Table 5.

Trim Procedure The multibody approach to the simulation of sophisticated mechanical systems may incur in problems related to its generality. In fact, as opposed to dedicated formulations, often an excessively detailed model is required even when most of the details are not essential. This is the case when a helicopter model in free flight must be analyzed even if only the details related to a limited portion of the model, e.g. the landing gear or the rotor dynamics, are of interest.

As the complexity of the model grows, the determination of a trimmed solution for a rotating rotor or for a steady landing gear deflection may require running a simulation for hundreds if not thousands of time steps. In fact, while a steady solution is usually dominated by the slow dynamics of the problem, a very detailed model exhibits high frequency transients, especially when integrated starting from untrimmed initial values.

Numerical Results

Two main problems were considered: a FAR/JAR 29 reserve energy landing following a vertical descent, and the oscillations of a helicopter on the ground.

Reserve Energy Landing

The condition considered for reserve energy landing was chosen with reference to the current regulations (FAR/JAR 29). A drop height of 13 in. (about 0.33 m), slightly above the reserve energy landing gear certification condition, corresponding to a drop test height of 1.5 times the limit height (12 in., resulting in about 0.30 m) was used in order to define the vertical speed at touchdown (2.5 m/s). A rotor thrust of 1.5 times the limit condition (2/3 of the maximum take-off weight) was used, resulting in full weight compensation. A drop of the helicopter without aerodynamic forces is considered first, to obtain reference ground loads; no gravity is included, to recreate complete weight compensation.

Model Constraints The model is constrained by forc-

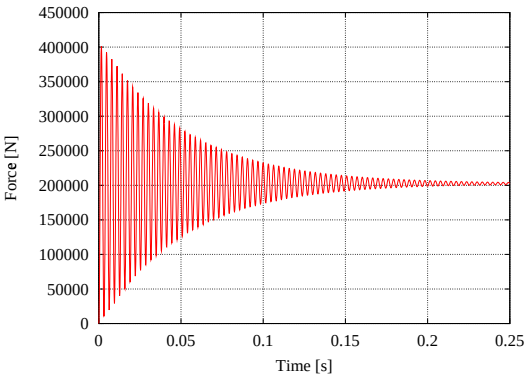

Figure 8: Blade axial load during simulation startup

ing the helicopter center of mass to move along a vertical line, allowing only the pitch rotation. The trimming of the tail rotor force is thus avoided. In fact, during the trimming transient, large changes in rotor thrust take place, eve though for limited periods of time, and this would unneccessarily complicate the modeling of the tail rotor force. On the other hand, it is reasonable to assume that the effects of the constraint on the loads both in the rotor and in the landing gear are negligible. Since the full thrust is established only after a short transient, during which the rotor reaches the trimmed cone and lag angles, a force that compensates the missing thrust during this transient is added to balance the weight.

Analysis Procedure The analysis starts with the rotor rotating at the nominal rotation speed; since the rotor is not trimmed, this results in a transient that exhibits a remarkable flapping motion from zero to the average cone angle. The startup also requires the flexible blades to reach a steady solution with respect to the axial load due to the centrifugal forces. This results in a very fast transient, because the axial stiffness is very high; however, since a short time step (1.e−4 s), required by the fast dynamics of the subsequent interaction with the terrain, is used, the axial straining of the blade is captured accurately, as shown in Figure 8. This is a clear example of how an over-detailed model, subjected to non physical initial values such as those of an untrimmed startup, may lead to spurious results that must be artificially damped. In the present case, this effect is obtained by means of large structural damping on the blade axial strain, which does not affect the rest of the analysis since the axial loads are nearly constant.

At the same time, the whole helicopter accelerates downwards, until the thrust balances the weight, reaching about 2.5 m/s, with only a limited overshooting. A substantially trimmed condition is reached in about two seconds, corresponding to 20,000 time steps, which require about 14 minutes on a Pentium III 600 MHz for a model with more than 800 degrees of freedom. To speed up the procedure, a parallel solution implementation was investigated, which is detailed in [8].

The helicopter is in a nearly trimmed axial descent flight condition when the landing gear hits the terrain. The contribution of the vertical velocity to the actual blade angle of attack determines a decrease in lift. For a fixed wing aircraft, this decrease can be significant (the lift may drop to more or less 1/3 of the aircraft landing weight). In the case under analysis, the thrust drop after landing with a touchdown vertical speed of 2.5 m/s is only about $1/10^{\text{th}}$ of the helicopter weight, because the mean induced velocity of the rotor during descent is about 18 m/s. As a consequence, the vertical speed is a small fraction of the downwash, and its effect on the total thrust is limited. Notice, however, that the ground effect was not considered in the present work: its contribution should diminish the induced velocity of about $1/5^{\text{th}}$, according to [19]:

$$u = u_\infty \left(1 - \left(\frac{R}{4z}\right)^2\right)$$

where z, 5.0 m at touchdown, is the height of the hub with respect to the ground, thus emphasizing the lift reduction effect. The figure is substantially unchanged according to more recent formulations and approximations [20].

As a consequence of the pitch degree of freedom, the MLG may hit the ground earlier than the NLG, resulting in a load distribution that differs from the ideal case of separate component drop tests. Figure 9 compares the ground loads during touchdowns of the complete system at different attitudes (0 deg, corresponding to a three point landing, and 5 deg) in absence of aerodynamic forces; no gravity was considered to emulate the full thrust compensation of the analyses in air. A pitch attitude angle of about 2.5 deg is reached at touchdown during the analyses with aerodynamic forces. After the simulations in air were performed, the drop in absence of rotor dynamics and aerodynamic forces was repeated with the same pitch attitude at touchdown; results are compared in Figure 10. Figure 11 shows the internal forces at different stations along the blade after the touch down; note the rebound and the second touchdown after about 3.5 s.

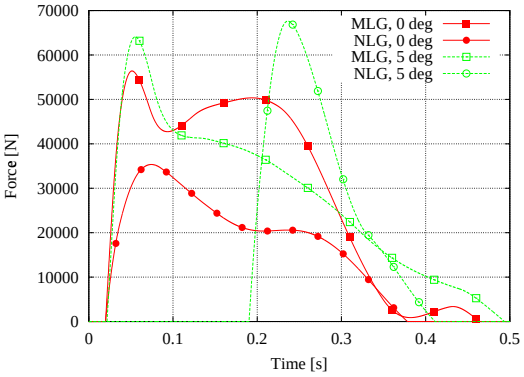

Figure 9: Tire vertical forces at 0 and 5 deg pitch attitude for a rotorless model

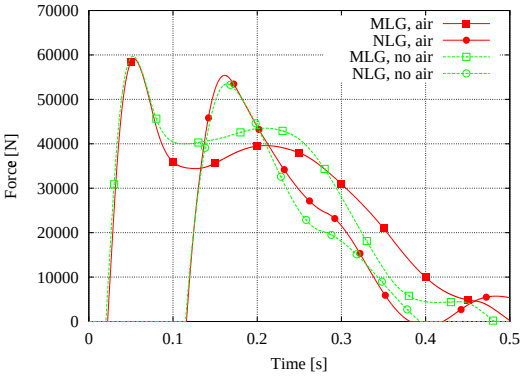

Figure 10: Tire vertical forces at 2.5 deg pitch attitude for a model with and without rotor aerodynamics

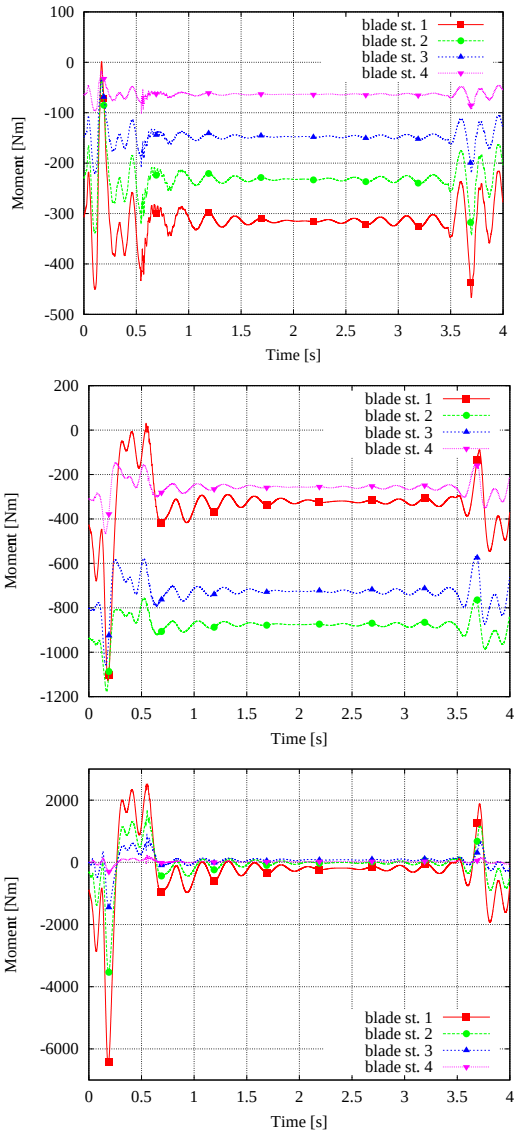

Figure 11: Blade internal moments after touchdown; blade stations are 1: $1/16^{\text{th}}$; 2: $5/16^{\text{th}}$; 3: $9/16^{\text{th}}$; 4: $13/16^{\text{th}}$ of blade radius. From top to bottom: torsional moment, out-of-plane bending (flapwise), in-plane bending (chordwise)

Ground Oscillations

The same model considered above is analyzed when resting on the landing gear, with the rotor rotating at the nominal rotation speed. Rotor wind-up and rotor brake maneuvers can be simulated as well, including effects such as the flexibility of the ground, an imposed movement of the ground itself (e.g. the deck of a ship in rough sea), imposed airflow and wind gusts; none of these effects are considered at present. Different rotor lead-lag damper characteristics are investigated to verify the sensitivity of the system to ground resonance problems. The effects of rotor aerodynamics on the stability and response of the helicopter are also addressed. Notice, however, that the aerodynamic forces used in the simulations, as previously mentioned, are formulated in a rather simplified manner, which misses many wake and blade-vortex interaction phenomena that can be particularly significant in hover. The analysis presented does not pretend to discuss in an exhaustive manner the stability of rotorcraft on flexible supports, or the ground resonance phenomenon. It rather addresses the possibility of analyzing sophisticated transients in a detailed manner.

Model Constraints The model is completely free; the longitudinal and lateral forces of the tires preserve the horizontal equilibrium and inhibit large displacements. The simplified tail rotor balances the main rotor torque. The vertical forces of the tires react the weight of the helicopter, while some thrust, about 10% of the weight, is present.

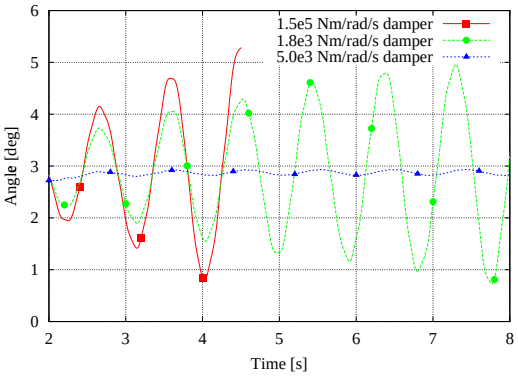

Figure 12: Blade lag angle for different blade damping properties in air

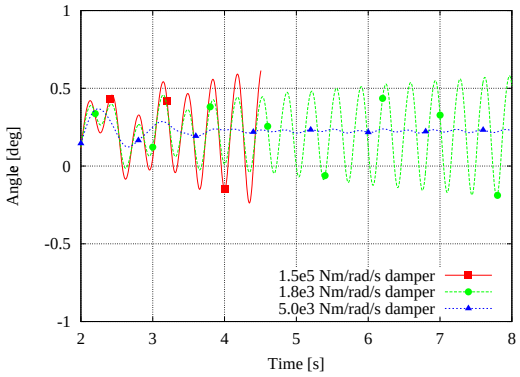

Figure 13: Helicopter pitch attitude angle for different blade damping properties in air

Analysis Procedure The analysis starts with the helicopter resting on the landing gear and the rotor rotating at the nominal speed. The system is not far from a trimmed condition, so when the system is stable, a steady solution is reached very quickly. The following cases are considered:

- sensitivity to blade lead-lag damper properties applied to the rotor rotating in air;
- sensitivity to blade lead-lag damper properties applied to the rotor rotating in vacuum;
- failure of one lead-lag damper in air.

Other analyses may be of interest:

- sensitivity to shock absorber damping properties in the vicinity of the landing gear static position;
- sensitivity to rotor rotating velocity;
- sensitivity to helicopter pitch and roll frequencies;

they have not been considered in this work.
The sensitivity of the system to the damping properties of the blade lead-lag dampers has been investigated first. Figure 12 shows the blade lag angle during the transient with different values of lead-lag damping. Figures 13-14 show the helicopter pitch and roll angles in the same cases. Note that the motion in the unstable case is dominated by the blade lag mode at about 0.8 Hz; the helicopter motion is dominated by the retreating lag motion, which is slightly above 3.0 Hz, the roll frequency. The simulation did not converge for extremely low damping coefficients.
There might be some dependence of the system stability on the modeling of the aerodynamic forces; it is common practice to neglect the aerodynamic forces in ground resonance investigations. Figure 15 shows the blade lag angle resulting from analyses with blade

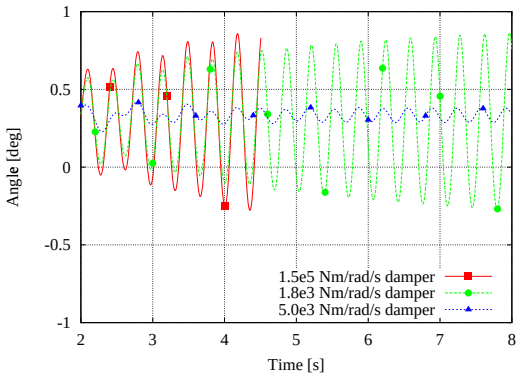

Figure 14: Helicopter roll angle for different blade damping properties in air

damper coefficients that result in stable transients in air; however, with the lowest blade damping coefficient, the system is unstable in vacuo. Figures 16-17 show the helicopter pitch and roll angles in the above mentioned cases. Despite the limits in the aerodynamic model considered in this analysis, the simulations in vacuo seem to be overconservative with regard to the stability of the system in ground resonance investigations.
The multibody analysis allows to introduce system perturbations like blade damper failures, resulting in rotor anisotropies. These off-design configurations can hardly be analyzed in an analytical form or even by means of comprehensive rotorcraft analysis codes. Figure 18 shows the lag angles of the rotor blades after a failure in the blade 1 damper. The motion of the failed blade is compared to that of another blade in the same case and to that of a blade in a reference rotor without failure. It is interesting to note, from Figure 19, the 1/rev perturbation that appears in the blade flap angle, due to the anisotropy of the rotor after the failure occurs. Figures 20-21 show the

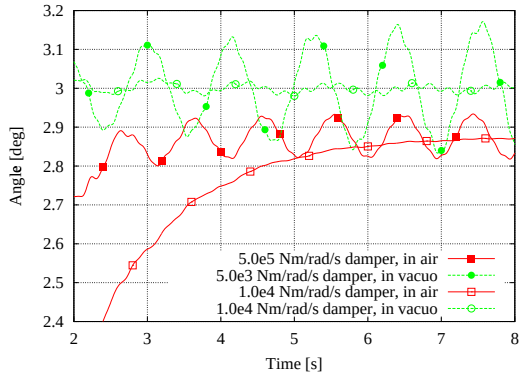

Figure 15: Blade lag angle for different blade damping properties in air and in vacuo

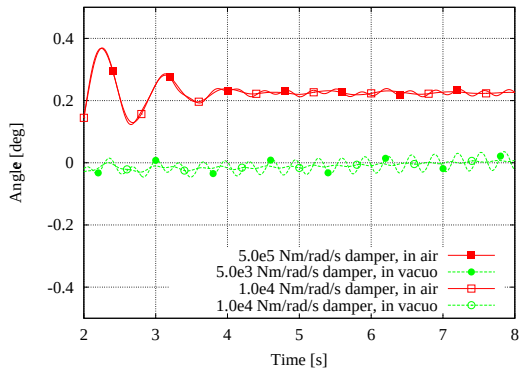

Figure 16: Helicopter pitch attitude angle for different blade damping properties in air and in vacuo

helicopter pitch and roll angles in the same situation.

Concluding Remarks

The paper discussed the use of a multibody analysis tool to investigate helicopter maneuvers involving the interaction with the terrain. A framework for the integrated modeling of complex, sophisticated systems was presented. The formulation of the landing gear components was discussed, based on previous works on landing gear dynamics of fixed wing aircraft. A model of a medium weight helicopter was presented and discussed; the entire main rotor dynamics and aerodynamics were modeled, together with detailed main and nose landing gears. A simplified model of the airframe and of the tail rotor was considered, without diminishing the generality of the approach. Two significant cases were investigated: a vertical reserve energy landing, and the free oscillations of the helicopter on the ground, with different trim conditions and different rotor lead-lag damping properties. The

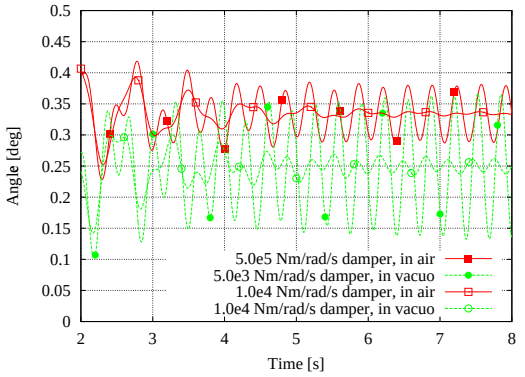

Figure 17: Helicopter roll angle for different blade damping properties in air and in vacuo

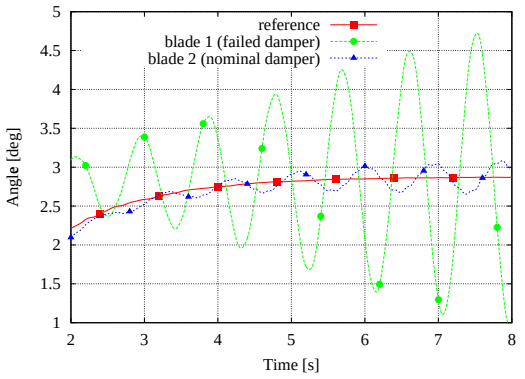

Figure 18: Blade lag angle for a failure in the blade 1 lead-lag damper

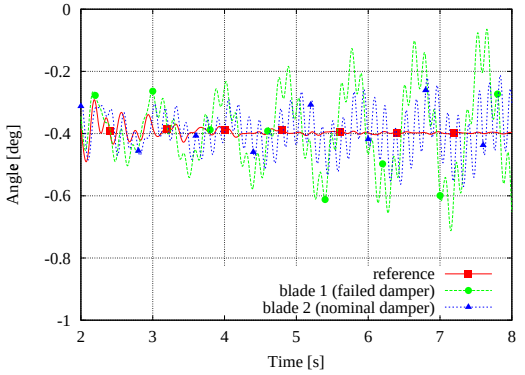

Figure 19: Blade flap angle for a failure in the blade 1 lead-lag damper

work addressed the feasibility of multibody, multidisciplinary analysis of complex, sophisticated systems including rotor dynamics, aerodynamics and landing gear analysis.

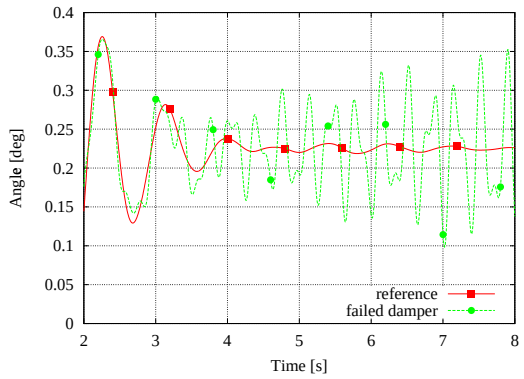

Figure 20: Helicopter pitch attitude angle for a failure in the blade 1 lead-lag damper

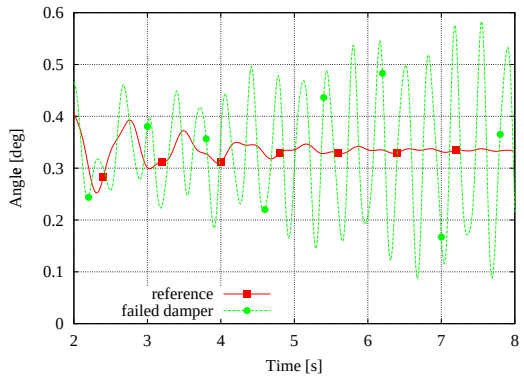

Figure 21: Helicopter roll angle for a failure in the blade 1 lead-lag damper

Acknowledgments

The Authors acknowledge the contributions of Prof. Lanz and Mantegazza and of Mr. Quaranta to the development of the multibody formulation.

References

[1] Olivier A. Bauchau and N. K. Kang. A multibody formulation for helicopter structural dynamic analysis. *Journal of the American Helicopter Society*, 38(2):3–14, April 1993.

[2] Gian Luca Ghiringhelli, Pierangelo Masarati, Paolo Mantegazza, and Mark W. Nixon. Multi-body analysis of a tiltrotor configuration. *Nonlinear Dynamics*, 19(4):333–357, August 1999.

[3] Leandro Girola. Simulazione del fenomeno di "ground resonance" con tecniche multi-corpo (Simulation of the ground resonance phenomenon by multibody analysis techniques). Master's thesis, Politecnico di Milano, Milano, Italy, 1993–94. in Italian.

[4] H. Wentscher, W. Kortüm, and W. Krüger. Fuselage vibration control using semi-active front gear. In *The Design, Qualification and Maintenance of Vibration-Free Landing Gear*, Banff, Canada, October 1995. AGARD.

[5] W. Krüger, I. Besselink, D. Cowling, D. B. Doan, W. Kortüm, and W. Krabacher. Aircraft landing gear dynamics: Simulation and control. *Vehicle System Dinamics*, 28(2–3):119–158, 1997.

[6] M. Boschetto, R. Bianco Mengotti, G.L. Ghiringhelli, and S. Gualdi. Analysis of landing gear behaviour for trainer aircraft. In 15^{th} *European ADAMS Users' Conference*, Rome, Italy, November 15–17 2000.

[7] Alvin Fong. Ground loads with a whole-aircraft model using ADAMS. In *North American MDI Users' Conference 2001*, Novi, Michigan, June 19–20 2001.

[8] Giuseppe Quaranta, Pierangelo Masarati, Massimiliano Lanz, Gian Luca Ghiringhelli, Paolo Mantegazza, and Mark W. Nixon. Dynamic stability of soft-in-plane tiltrotors by parallel multibody analysis. In 26^{th} *European Rotorcraft Forum*, pages 60.1–9, The Hague, The Netherlands, 26–29 September 2000.

[9] Pierangelo Masarati, Gian Luca Ghiringhelli, Massimiliano Lanz, and Paolo Mantegazza. Integration of hydraulic components in a multibody framework for rotorcraft analysis. In 26^{th} *European Rotorcraft Forum*, pages 57.1–10, The Hague, The Netherlands, 26–29 September 2000.

[10] GianLuca Ghiringhelli and Mario Boschetto. Design landing loads evaluation by dynamic simulation of flexible aircraft. In *AGARD CP-484 Landing Gear Design Loads*, Povoa de Varzim, Portugal, October 8–12 1990. AGARD.

[11] B. Milwitzky and F. E. Cook. Analysis of landing gear behavior. TR 1154, NACA, 1954.

[12] Part 29: Transport category rotorcraft. In *Federal Aviation Requirements*, Airworthiness Standards. FAA.

[13] Part 29: Large rotorcraft. In *Joint Aviation Requirements*, Airworthiness Standards. JAA.

[14] Robert F. Smiley and Walter B. Horne. Mechanical properties of pneumatic tires with special reference to modern aircraft tires. TR R-64, NASA, 1960.

[15] Frictional and retarding forces on aircraft tyres. In *ESDU*, volume 5 of *Performance*. ESDU, 1971.

[16] H. Sakai. Theoretical and experimental studies on the dynamic properties of tyres, part 3: Calculation of the six components of force and moment of a tyre. *International Journal of Vehicle Design*, 2(3):335–372, 1981.

[17] Gwanghun Gim and Parviz Nikravesh. An analytical model of pneumatic tyres for vehicle dynamics simulations. part 3: Validation against experimental data. *International Journal of Vehicle Design*, 12(2):217–228, 1991.

[18] Gian Luca Ghiringhelli, Pierangelo Masarati, and Paolo Mantegazza. A multi-body implementation of finite volume beams. *AIAA Journal*, 38(1):131–138, January 2000.

[19] I. C. Cheeseman and N. E. Bennett. The effect of ground on a helicopter rotor in forward flight. TR 3021, NASA, 1955.

[20] J. Gordon Leishman. *Principles of Helicopter Aerodynamics*. Cambridge University Press, Cambridge, UK, 2000.